EXAFS and XRD studies in synthetic Ni-Fluorohectorite

Leander Michels[1], Luciano Ribeiro[2,*], Maria Suely Pedrosa Mundim[3], Marcelo Henrique Sousa[4], Roosevelt Droppa Jr.[5], Jon Otto Fossum[1,*], Geraldo José da Silva[3], Kleber Carlos Mundim[6],

[1]Department of Physics, Norwegian University of Science and Technology – Trondheim, Norway
[2]Unidade Universitária de Ciências Exatas e Tecnológicas, Universidade Estadual de Goiás, 75.132-903,Anápolis– GO, Brazil
[3]Instituto de Física, Universidade de Brasília, 70.919-970, Brasília – DF, Brazil
[4]Faculdade de Ceilândia,Universidade de Brasília, 72.220-140, Brasília – DF, Brazil
[5]Universidade Federal do ABC, 09.210-580, Santo André – SP, Brazil
[6]Instituto de Química, Universidade de Brasília,70.904-970, Brasília – DF, Brazil

*Corresponding author: E-mail address: lribeiro@ueg.br
jon.fossum@ntnu.no

ABSTRACT

In the present work the synthetic clay mineral fluorohectorite was studied by means of extended X-ray absorption fine structure (EXAFS) in a powder sample with the intention to observe the number of neighbouring atoms to the Ni interlayer cation. In addition X-ray Diffraction (XRD) was performed in order to follow the hydration states of Ni-fluorohectorite in terms of basal-spacing measurements. The sample conditions were the same for both types of experiments. The EXAFS results show that Ni^{2+} forms a Brucite-like structure in the form of $Ni(OH)_2$, and that this structure coexists with the clay mineral particles. This shows that the Ni atom observed by means of our EXAFS measurements is predominantly the Ni which composes the Brucite-like structure and not the interlayer Ni^{2+} cation. In order to confirm the formation of the Brucite-like structure, the EXAFS data from Ni-fluorohectorite were compared to Ni-salt water solutions at various pH.

Highlights

1. Investigation of the water solvation process around the intercalated Ni^{2+} cation;
2. Simultaneously in-situ X-ray absorption (EXAFS) and scattering techniques (XRD);
3. Simultaneous control of temperature and relative humidity.

Keywords

1. Synthetic Clay Mineral Ni-Fluorohectorite;
2. Temperature;
3. Relative Humidity;
4. EXAFS;
5. XRD.
6. Brucite

Graphical Abstract

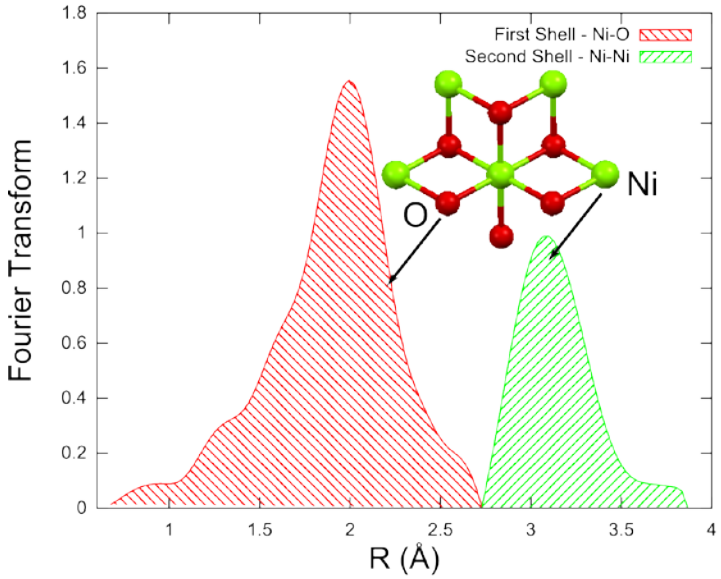

1. Introduction

The ability of the smectites to absorb molecules into their interlayer space is well known. The swelling property, which is resultant of interactions between these molecules and the clay mineral itself, has attracted the interest of many scientists, and it is important in a wide number of clay mineral based applications. For example, in a recent study, molecules of CO_2 could be intercalated at specific values of pressure and temperature (Hemmen et al., 2012), which is important for CO_2 storage. In another study, important in drug delivery applications, it was demonstrated that it is possible to intercalate tetracycline into Laponite (Ghadiri et al., 2013). However, one of the most studied, although not yet completely understood complex system, is the interaction between water and the clay mineral. The process of water intercalation is highly dependent on the interlayer cation as well as on the layer charge (Dazas et al., 2013; Gates, 2006; Gates et al., 2012) and it has been studied by many techniques such as X-ray diffraction (XRD) (Wada et al., 1990), X-ray absorption fine structure (XAFS) (Ashley and Doniach, 1975; Lee and Beni, 1977; Lee and Pendry, 1975; Schaich, 1973), nuclear magnetic resonance (NMR) (Tenorio et al., 2010, 2008) and Quasi-elastic Neutron Scattering (QENS) (Bordallo et al., 2008; Gates et al., 2012).

XRD gives information about the interplanar distances of the (001) basal planes. However, the details about the behaviour of the intercalated components such as cations and its solvation layers cannot be obtained from XRD. Other methods, such as extended X-ray absorption fine structure (EXAFS), must be used to obtain complementary information of such processes. The EXAFS method uses the interlayer cation itself as a probe.

The synthetic clay mineral fluorohectorite, used here, has chemical nominal formula per half unit cell M_x–$[Mg_{(3-x)}Li_x]Si_4O_{10}F_2$, where M refers to the type of intercalated cation, which is known to substantially influence the physical-chemical behaviour of the system. Hectorite is a 2:1 phyllosilicate, meaning that the layers are formed by two inverted silicate tetrahedral sheets, sharing their apical oxygen with one octahedral sheet sandwiched in between. It is classified as a trioctahedral smectite since Li^+ substitute for Mg^{2+} in the octahedral sheet sites, which are fully occupied. The proportion x of the Li^+ ions determines the surface charge of the layers, which are

held together in the stacked structure by sharing the interlayer cations. During the past decade several works have been published on Na-fluorohectorite (Na-Fh) (da Silva et al., 2003, 2002; Hansen et.al., 2012; Tenorio et.al. 2008) and Li-fluorohectorite (Li-Fh) (Michels et al., 2012; Tenorio et al., 2010).

In the present manuscript we have studied Ni-fluorohectorite, which is regarded as a representative clean model system of natural smectites, by means of XRD and EXAFS. Ni has an absorption edge of 8333 eV well suited for EXAFS studies. It was previously reported that Ni^{2+}, in aqueous solution, has water coordination dependent on the pH. In the case of a basic solution, it is known that the first and second coordination shells are formed by O and Ni with respective distances of ~2.05 Å and ~3.2 Å (Ribeiro et al., 2011, 2007; Sandstrom et al., 1977).

The purpose of the present work was to perform EXAFS measurements on Ni-fluorohectorite in a range of temperatures in order to observe changes in the first and second coordination shells of the Ni^{2+}, while simultaneously performing XRD measurements to verify the interlayer spacing in the (001) direction during the water intercalation process. The simultaneous in-situ use of both techniques can allow us to investigate the hydration states of the clay mineral and the surroundings of Ni^{2+} at a given temperature and relative humidity. With such an experimental approach we can improve the reliability of the water intercalation studies since it connects distinct information, from two different experimental points of views, for the same physical process.

2. Materials and Methods

2.1. Sample and experimental setup

The samples were prepared by cationic exchange starting from Li-fluorohectorite in a three months dialysis procedure as described elsewhere (Løvoll et al., 2005). The pH was measured to be 9.5 during the cation exchange process and this was adjusted by the clay itself.

After the cation exchange process, the dried Ni-fluorohectorite powder samples were placed in a specially designed cell, as shown in Fig. 1. The temperature was controlled by using a thermal bath and Peltier element connected to the cell. The temperature range was from 5 to 125 °C, in order to avoid the temperatures in which the Hofmann-Klemen effect occurs (Hofmann and Klemen, 1950; Komadel, 1999; Komadel et al., 2005). Briefly, this effect is the migration of the interlayer cation into the clay mineral layer at temperatures above 200 ºC. The relative humidity was monitored with a Sensirion SHT15 Humidity and Temperature sensor placed inside the cell. Tests were done before the experiments in order to determine the optimized sample thickness for EXAFS experiment.

The experiments were carried out varying the temperature in two different conditions: (1) in a completely dry environment, with relative humidity RH = 0 %, and (2) with the samples in the presence of humidity.

In the first case, the temperature were scanned from 20 °C to 125 °C, in steps of 5 °C, keeping the RH at 0 % along the scan. In the second case, the measurements were performed in the temperature range between 5 °C and 65 °C in steps of 10 °C. The RH was varied by circulating

humidified air through the cell shown in Fig. 1. In both cases the time interval between each temperature step was ~ 20 minutes for the system stabilization.

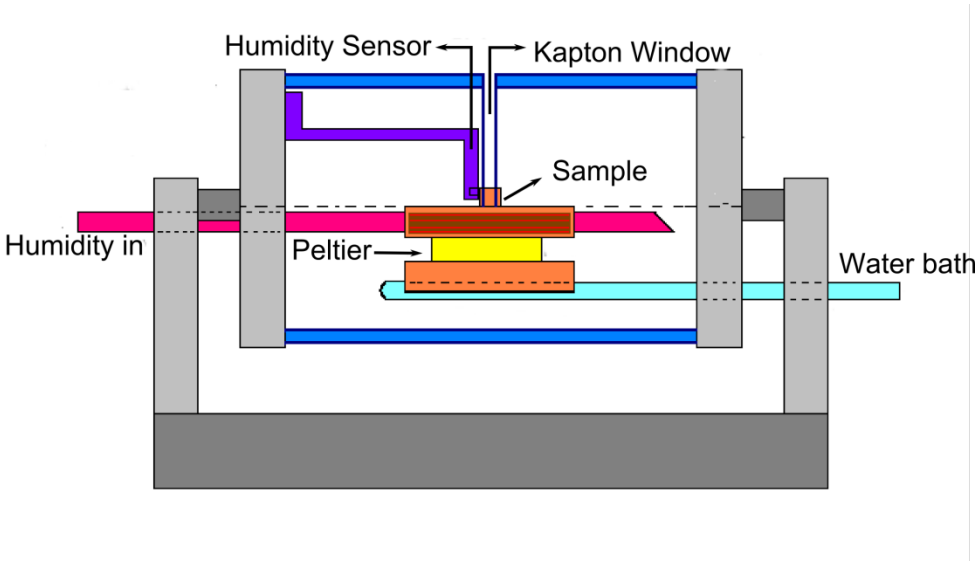

Figure 1- Side view of the sample cell showing the water bath, humidity and the Peltier element.

2.2. EXAFS data collection and analysis

EXAFS data at the Ni K edge were collected on beamline D04B at the Brazilian Synchrotron Light Laboratory - LNLS, Campinas - SP, Brazil. It is equipped with a Si (111) channel cut monochromator calibrated at the inflexion point of the absorption edge for the pure element Ni (8333 *e*V), obtained by transmission (Tolentino et al., 1998, 2001). The spectra were taken, approximately, from 200 *e*V below the edge to 1000 *e*V above the edge. The experimental data were normalized by the intensity of the last point in energy and compared with the spectra of the Ni standard sample.

For background subtraction and data fitting, the softwares ATHENA and ARTEMIS (Ravel and Newville, 2005) were used. Individual spectra were averaged and subsequently corrected for background absorbance and normalized. Data analysis was carried out in the standard way described in (Elam, 1989). The scans were aligned with the reference spectra and merged in energy space. Pre-edge background was removed and spectra normalized to a step height of 1. The edge energy E_0 was chosen at the inflection points of the absorption edges. The post-edge background was removed to isolate the EXAFS oscillations in the energy space $\chi(E)$. The data were then transformed to wave number space $\chi(k)$ in the range from 0.0 to 15.0 $Å^{-1}$. Fourier transformation of the raw $k^2\chi(k)$ function (Sayers et al., 1971) was performed in the interval $2.0 < k < 14.0$ $Å^{-1}$ to obtain a radial structure function. In this process, it was used a Kaiser-Bessel window function with width 2.0.

Characteristic EXAFS spectra are modelled by (Lee and Pendry, 1975)

$$\chi(k) = \sum_i \frac{N_i S_0^2(k) F_i(k)}{kR_i^2} e^{-2k^2\sigma^2} e^{-R_i/\lambda(k)} \, sin[2kR_i - \delta_i(k)], \qquad (1)$$

where $F_i(k)$ is the effective scattering amplitude, $\delta_i(k)$ is the phase shift, $\lambda(k)$ is the mean free path of the scattered photoelectron, S_0^2 is the electrons reduction factor, R_i is the distance to the neighboring atom, N is the number of neighbouring atoms, and σ is the disorder in the neighbours distances (Debye-Waller factor).

2.3. XRD data collection and analysis

The simultaneous XRD measurements (at beamline D04B at LNLS as described above) were performed for the case in which RH was different from zero. The experimental procedure consisted in fixing the X-ray beam energy at 200 *e*V below the Ni absorption edge (8.333 k*e*V) for the acquisition of 2D diffractograms by using an image plate. The experimental setup sketch is shown in Fig. 2.

The basal spacing of layers was determined from Bragg's equation, written in the form,

$$d_{basal\ spacing} = \frac{\lambda}{2\ \sin\left[\frac{1}{2}\tan^{-1}\left(\frac{1}{2}\frac{N_p \cdot S_p}{d_{SD}}\right)\right]} \qquad (2)$$

where λ is the X-ray wavelength, N_p is the number of pixels and S_p is the pixel size (0.2 mm), and d_{SD} is the sample to detector (image plate) distance, set to 290 mm during the experiments.

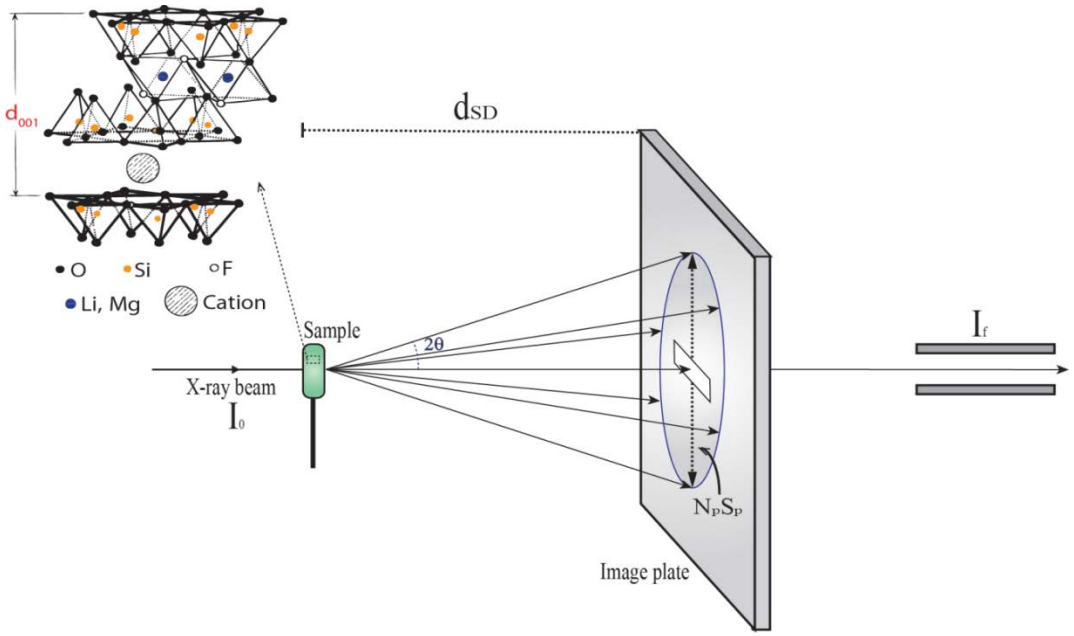

Figure 2- A representative illustration of the setup of XRD (Eq. (2)) and EXAFS experiments (I_f/I_0).

4. Results

4.1 EXAFS

The k^2-weighted EXAFS spectra for Ni-fluorohectorite taken at some temperatures in dry environment and in the presence of humidity are shown in Fig. 3(a) and Fig. 3(b) respectively. In

Fig. 4, the respective Fourier transform are presented. These data were treated according to the procedures described in the section 2.2.

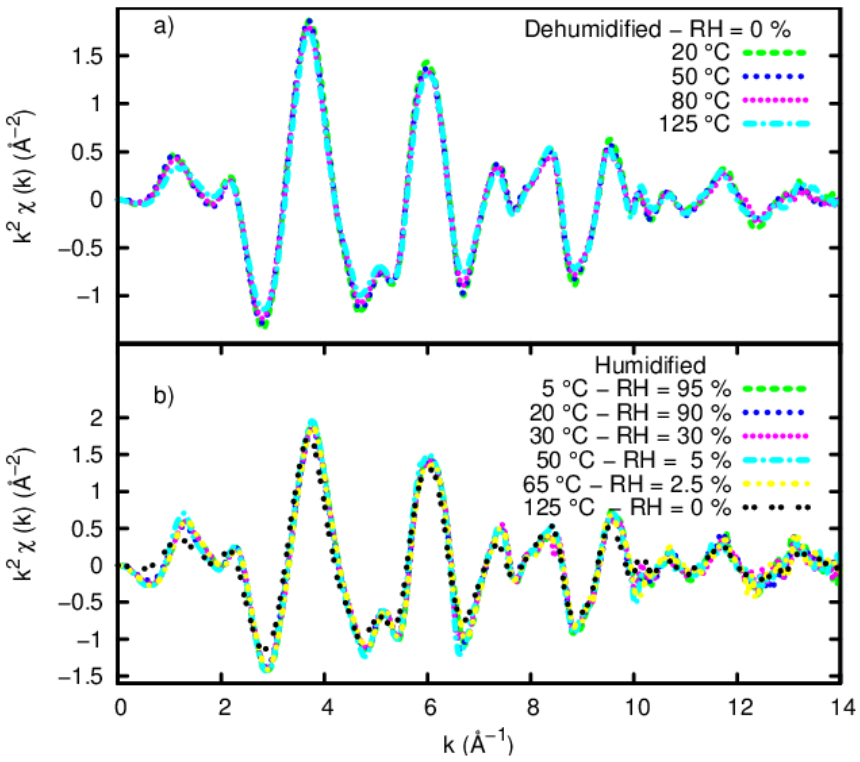

Figure 3 - k-space EXAFS spectra of (a) dehumidified and (b) humidified Ni-fluorohectorite samples.

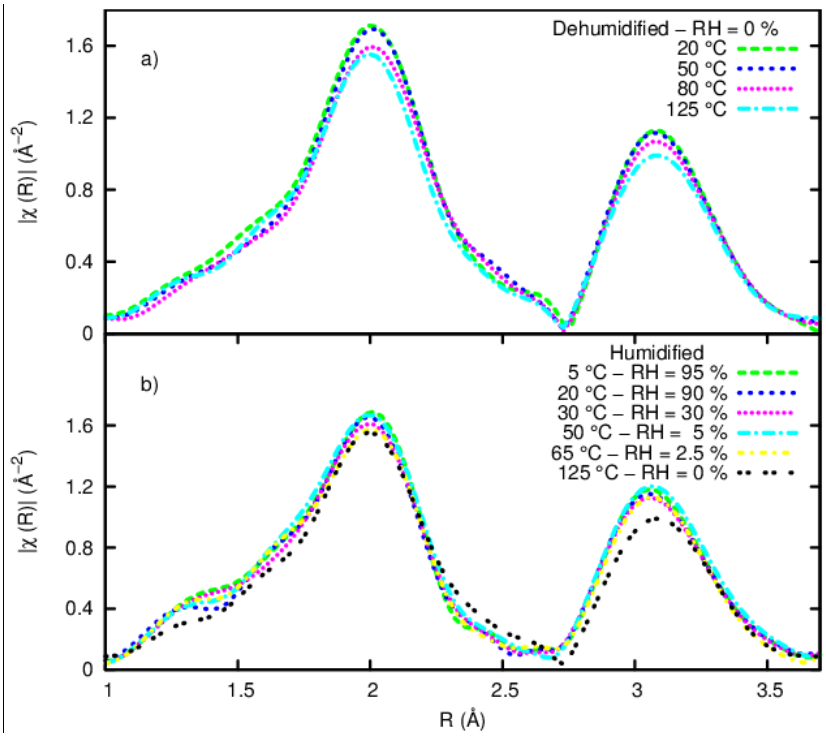

Figure 4 - Fourier transform of the EXAFS spectra of (a) dehumidified, RH = 0 % and (b) humidified RH ≠ 0 % Ni-fluorohectorite samples. The FT was done by using Kaiser-Bessel apodization type within the range of 2.40 to 14.0 Å^{-1}.

Comparing the spectra in the Figures 4(a) and 4(b), it is observed that amplitudes decrease with increasing temperature while the average distances between the Ni atom and its neighbours

remain unchanged. This means that in the EXAFS equation, shown in Eq. (1), the parameters that define temperature dependence of the EXAFS signal amplitude, are *N*, which represents the number of neighbour atoms (which can change in presence of water molecules), and σ, which represents the thermal motion of the atoms. So the reduction of the EXAFS amplitude can be either due to the decrease of the number of neighbour atoms, or due to the effects of thermal motion represented by the Debye-Waller factor.

Fig. 4(a) shows that the EXAFS amplitude decreases as temperature increases. In this experiment the only parameters in the EXAFS amplitude, shown in Eq. (1), which were varied, are *N* and σ. Since RH = 0 % means that there no water molecules present, it is expected that *N* remains constant, therefore the variation of the EXAFS amplitude can only be attributed to the thermal motion of the atoms, represented by the Debye-Waller factor σ. On the other hand, Fig. 4(b) shows a similar behaviour even when the RH is changed. Thus the existence of both peaks and the similarities in between Fig. 4(a) and Fig. 4(b) cannot be justified by attributing it to the presence or absence of water molecules. If the peaks were related to the first and second water coordination shells (Dähn et al., 2002; Manceau et al., 2003), they should significantly change when temperature reaches 125 ^{o}C, since there would not be any water molecule in the interlayer space at this temperature, which was not observed as shown in Fig. 4 (a).

4.2 XRD

In order to monitor the clay mineral hydration states, XRD experiments were performed simultaneously with EXAFS, as described in section 2.3. The RH was measured while the temperature was changed in an interval between 5 ^{o}C and 125 ^{o}C, as shown in Fig. 5. Fig. 5(a) presents the photographic film after five minutes exposition to the diffracted radiation of the sample powder. Fig. 5 (b) illustrates the diffraction cones at temperatures of 20 °C, 50 °C and 125 °C, with relative humidity, of respectively 85 %, 50 % and 0 %, and the basal spacing, respectively, 18.4 Å, 13.9 Å and 11.7 Å. Fig. 5(c) shows the curve of the change in spacing between the layers as a function of temperature. Table 1 shows the average interlayer spacing of the Ni-Fh for different temperature and RH intervals.

Table 1 - Interlayer spacing of the clay mineral for different temperature ranges.

Temperature Range (°C)	Relative Humidity (%)	Basal distance (Å)
09	95	18.63
20	90	18.47
30	30	14.55
50	5.0	13.91
60	2.5	13.89
70	2.0	13.82
80	1.0	12.32
110	0.0	12.32

120	0.0	11.25
125	0.0	11.70

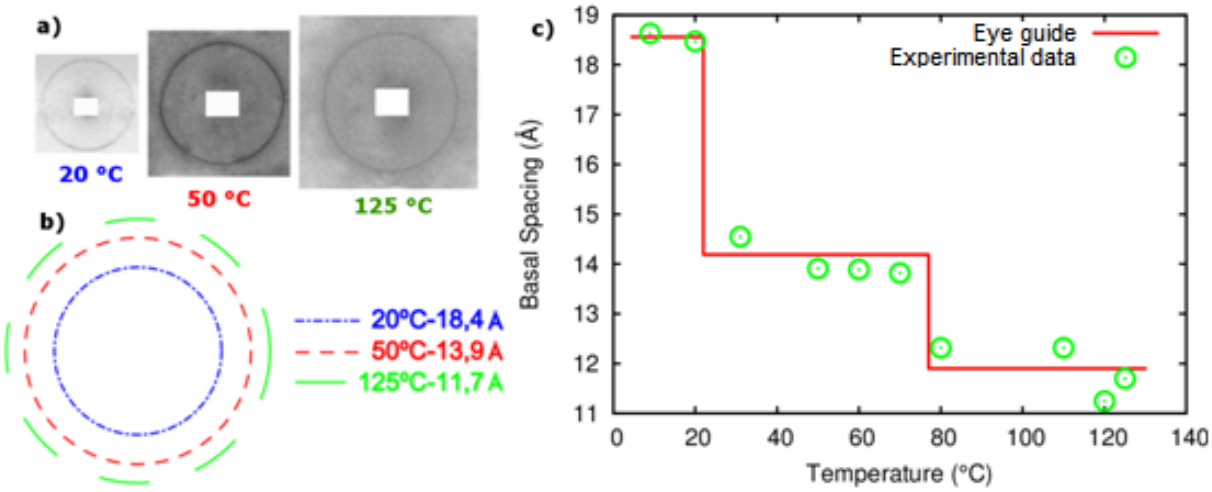

Figure 5–(a) Scattering of the Ni-fluorohectorite sample by XRD. (b) The circles represent the basal distances of the layers in Ni-fluorohectorite in the temperatures of 20°C, 50°C and 125°C, respectively and relative humidity of 85 %, 50 % and 0 %. (c) The data points represent the basal distance between the layers as function of temperature. The line identifies the clay mineral hydration states.

The XRD results, presented in Table 1 and Fig. 5, show evidence that there is a cation occupying the interlayer space of the clay mineral, since the basal spacing variation reveals the water intercalation, which is possible due the presence of an interlayer cation (in the present case Ni^{2+}) (Bordallo et al., 2008). Other related studies show that Ni-fluorohectorite has intercalated water layers (WL) quite well ordered along the stacking direction (Aalerud, 2001; Grassi et al., 2013). From Fig. 5(b), Ni-fluorohectorite clay mineral in the 0WL hydration state has a basal spacing of 11.7 Å at 125 °C. The 20 °C plateau gives a basal distance of the 18.4 Å which means a 3WL state of hydration. The basal spacing shown in Fig. 5(c) is in the same range as measures in previous works on Li-fluorohectorite (Tenorio et al., 2010) and Na-fluorohectorite (Hansen et al., 2012).

5. Discussion

The EXAFS result described above can be attributed to the formation of a crystal structure with chemical formula $Ni(OH)_2$ similar to Brucite-like (Curti et al., 2009; Dähn et al., 2002; Manceau et al., 2003; Pandya et al., 1990), during the dialysis process of cation exchange. It is assumed that the structure formed has two coordination numbers of Ni-O ~ 2.06 Å and Ni-Ni ~ 3.04 Å (Wang et al., 2004) and that this process is pH dependent. From Fig. 5 it is however clear that the presence of such a Brucite-like structure is not interfering with the swelling process, due to the water intercalation. From Fig. 4 it is possible to see the minimum size of the Brucite-like structure, which is ~ 3.5 Å. One can note that such a structure is too large to fit within the interlayer space. Thus one can assume that they are located in between the clay mineral particles, as suggested in Fig. 6.

The H^+ generated from the hydrolysis of the $Ni^{2+}\cdot 6(H_2O)$ was neutralized by the high concentration of OH^-, since the pH was measured during dialysis to be approximately 9.5, which means that there is not enough H^+ to fully counter the negative charge of the fluorohectorite layers (Kreit et al., 1982) since the concentration of protons is about 0.3 nanomoles. However one cannot exclude the possibility that some H^+ could coexist with Ni^{2+} in the interlayers.

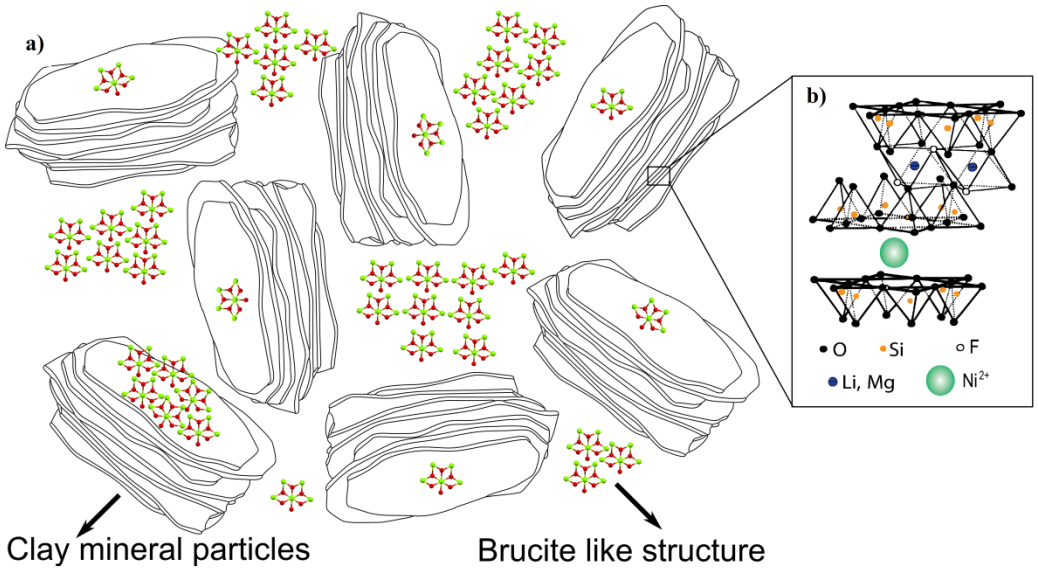

Figure 6 – a) Sketch of coexistence of clay mineral particles Ni-FH and the Brucite-like structure. The present experiments cannot distinguish details of the Brucite-like structures. b) Layer zoom of fluorohectorite showing the unit cell structure with Ni as an interlayer cation.

In order to verify the appearance of this Brucite-like structure, a salt solution of $NiCl_2\cdot 6(H_2O)$ with different pH values was prepared. An EXAFS spectrum was taken and compared with the spectra obtained from the Ni-fluorohectorite. The results are in Fig.7, which shows that in a basic pH there is a formation of a $Ni(OH)_2$ structure with two different coordination shells. In fact, taking into account the solubility product constant for the $Ni(OH)_2$, it is possible to predict that precipitation of nickel hydroxide starts at pH ~ 7 in a 0.1 mol/L Ni^{2+}solution, for example. The peak positions from the Ni solution with pH 7.77 are similar to those of hydrated Ni-fluorohectorite at 20°C, which was obtained with a dialysis procedure at pH approximately 9.5, set by the clay itself.

One can also observe that at the pH 7.77, a peak at ~3.1 Å, which corresponds to the second peak position of Ni-FH, appears. EXAFS studies of a Ni water solution, with pH in the same range, a crystalline structure similar $Ni(OH)_2$ to is formed (Pandya et al., 1990).

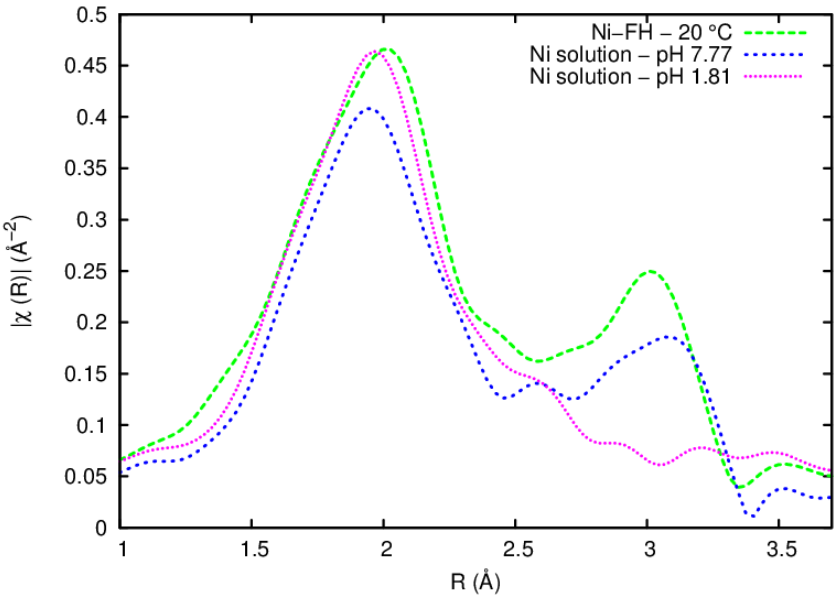

Figure 7. Comparison between the Fourier transformed spectra of Ni-FH and those of two Ni solutions with different pH values.

The quantitative analysis, of the data presented in Fig. 4 was done using the standard $Ni(OH)_2$ model. In this model Ni has 6 oxygen and 6 nickels in the first shell and second coordination shell respectively. The data fitting was performed using k^2-weighting. The software IFEFFIT (Newville, 2001; Ravel and Newville, 2005) were used to calculate theoretical phase and amplitude functions of Ni–O and Ni-Ni scattering paths using input files based on the structural crystalline $Ni(OH)_2$ (Ravel, 2001). A reduction factor S_0^2 with a value of 0.85 (O'Day et al., 1994) used in all fits.

In a previous study (Dähn et al., 2002) concerned with the process of Ni uptake in montmorillonite, the structural parameters, obtained within a period of 90 days, provide the coordination number (N) of the first shell $N_{Ni\text{-}O}$ equal 5.1 and the interatomic distance of the $Ni-O$ equal 2.04 Å. For the second shell it was found that $N_{Ni\text{-}Ni}$ and $R_{Ni\text{-}Ni}$ had values of 5.1 and 3.07 Å, respectively, which were reported previously for $Ni(OH)_2$ (Gräfe and Sparks, 2005; Gräfe et al., 2004; Pandya et al., 1990; Scheckel et al., 2000; Scheidegger et al., 1996; Scheinost and Sparks, 2000). This is typical of six fold coordinated Ni and based on these reports it was adopted both for $N_{O\text{-}Ni}$ and $N_{Ni\text{-}Ni}$ an idealized value of 6.

Following Fig. 4(a) an inverse FT was performed for the first coordination shell, within the interval of $\Delta R = 1.0 - 2.8$ Å. The fitting parameters were the radial distance (R, Å) and the Debye–Waller factor (σ^2, Å^2). The procedure for the second coordination shell was repeating the process done in the first shell but extending the ΔR interval to 3.8 Å. The results of these adjustments are shown in Table 2.

Table 2 - Curve fitting results of Ni K edge EXAFS spectra of the Ni-fluorohectorite for first and second coordination shells for the Fig. 4(a).

T (° C)	The first shell – Ni-O		The second shell – Ni-Ni	
	R_{Ni-O}(Å)	$\sigma^2(\times 10^{-3}$Å$^2)$	R_{Ni-Ni}(Å)	$\sigma^2(\times 10^{-3}$Å$^2)$
120	2.03 ± 0.10	6.2 ± 0.4	3.08 ± 0.03	9.9 ± 0.3
100	2.03 ± 0.10	6.1 ± 0.3	3.08 ± 0.03	9.1 ± 0.2
80	2.04 ± 0.09	5.8 ± 0.2	3.08 ± 0.04	9.3 ± 0.3
60	2.04 ± 0.09	5.5 ± 0.5	3.08 ± 0.04	8.9 ± 0.4
50	2.04 ± 0.09	5.7 ± 0.3	3.08 ± 0.04	8.9 ± 0.2
45	2.04 ± 0.09	5.2 ± 0.5	3.08 ± 0.04	8.5 ± 0.4
30	2.04 ± 0.09	5.5 ± 0.9	3.08 ± 0.03	8.2 ± 0.4
20	2.04 ± 0.09	5.3 ± 0.5	3.08 ± 0.03	8.5 ± 0.4

The Debye-Waller factor obtained previously for the dry case was kept fixed and the same values were used for the humid data fittings. The coordination number was also a parameter used to evaluate its behavior. The results of the adjustments are shown in Table 3.

Table 3- Curve fitting results of Ni K edge EXAFS spectra of the Ni-fluorohectorite in the presence of relative humidity for the first and second coordination shells, shown in Fig. 4(b).

T (° C)	The first shell – Ni-O		The second shell – Ni-Ni	
	N_{Ni-O}	R_{Ni-O}(Å)	N_{Ni-Ni}	R_{Ni-Ni}(Å)
5	5.9 ± 0.3	2.05 ± 0.09	5.7 ± 0.3	3.07 ± 0.03
20	5.9 ± 0.6	2.04 ± 0.09	5.6 ± 0.5	3.08 ± 0.03
30	5.8 ± 0.3	2.04 ± 0.09	5.4 ± 0.2	3.08 ± 0.03
45	6.1 ± 0.4	2.04 ± 0.09	6.1 ± 0.4	3.08 ± 0.03
50	6.2 ± 0.3	2.04 ± 0.09	6.3 ± 0.3	3.08 ± 0.03
65	6.4 ± 0.4	2.04 ± 0.09	6.3 ± 0.2	3.08 ± 0.03

The coordination number of the first and second shells has small oscillations around the number previously set for the dried case but within the uncertainties it can be considered constant and it does not reflect the water intercalation process observed in XRD. For the interatomic distances the values of $R_{Ni-O} \approx 2.04$ Å and $R_{Ni-Ni} \approx 3.08$ Å remain equal to the ones obtained for the dried case. Thus, the information contained in Tables 1 and 2 show that the same structure was present independently of whether the sample was dried or humidified.

6. Conclusion

In this work EXAFS measurement was performed as a function of temperature studying the synthetic Ni-fluorohectorite in two different situations of RH: Dry and humidified. Simultaneous in-

situ XRD measurements were performed in order to verify the clay mineral hydration states, using the (001) reflection, within a range of temperatures and RH.

The present EXAFS study indicates the presence of a structure similar to Brucite in the form of $Ni(OH)_2$. It is verified that the process of such a structure depends on pH, suggesting that it can be connected to the high pH characteristic of the Ni-fluorohectorite clay mineral. The water intercalation process measured simultaneously in-situ by XRD, cannot be directly observed as a dominant feature in the EXAFS measurements due to the presence of the Brucite-like structure. The observed Brucite-like structure is present both in dry and humid sample conditions, indicating Brucite-like formation during the cation exchange process for the Ni-fluorohectorite samples used in these studies. The present experiments do not provide an answer to wherein the sample the Brucite-like structures are located, whether they are attached to the clay mineral particles or distributed within the clay mineral particle powder, or both. The size of the Brucite-like structures does not allow them to fit inside the interlayer space of the clay minerals, in accordance with our XRD measurements. Since the hydrolysis produces protons, these protons can contribute to the neutralization of the negative charge of the fluorohectorite layers. Thus Hydrogen-fluorohectorite is produced and the change of the interlayer distance upon heating can be due to dehydration of Hydrogen-fluorohectorite.

A future work is to verify experimentally any presence of Hydrogen-fluorohectorite, and the Brucite-like structure. Future investigations should also include performing EXAFS as a function of relative humidity while keeping the temperature fixed. In this way the amplitude reductions in the EXAFS will be mainly attributed to changes in the coordination number.

Acknowledgments

The authors acknowledge the Brazilian Synchrotron Light National Laboratory (LNLS-CNPEM/MCTI) for the support on XAFS and XRD experiments. JOF appreciate support from the Research Council of Norway. Z. Rozynek is acknowledged for providing useful comments to the manuscript. We are indebted to Fabio R. Zambello for technical help.

References

Aalerud, T.N., 2001. Synchrotron X-ray Scattering Studies of Water Intercalation in Synthetic Smectite Nickel-Fluorohectorite. Norwegian University of Science and Technology (NTNU).

Ashley, C.A., Doniach, S., 1975. Theory of extended x-ray absorption edge fine structure (EXAFS) in crystalline solids. Phys. Rev. B 11, 1279–1288.

Bordallo, H.N., Aldridge, L.P., Churchman, G.J., Gates, W.P., Telling, M.T.F., Kiefer, K., Fouquet, P., Seydel, T., Kimber, S.A.J., 2008. Quasi-Elastic Neutron Scattering Studies on Clay Interlayer-Space Highlighting the Effect of the Cation in Confined Water Dynamics. J. Phys. Chem. C 112, 13982–13991.

Curti, E., Dähn, R., Farges, F., Vespa, M., 2009. Na, Mg, Ni and Cs distribution and speciation after long-term alteration of a simulated nuclear waste glass: A micro-XAS/XRF/XRD and wet chemical study. Geochim. Cosmochim. Acta 73, 2283–2298.

317 Da Silva, G., Fossum, J., DiMasi, E., Måløy, K., 2003. Hydration transitions in a nanolayered synthetic silicate: A
318 synchrotron x-ray scattering study. Phys. Rev. B 67, 094114.

319 Da Silva, G., Fossum, J., DiMasi, E., Måløy, K., Lutnæs, S., 2002. Synchrotron x-ray scattering studies of water
320 intercalation in a layered synthetic silicate. Phys. Rev. E 66, 011303.

321 Dähn, R., Scheidegger, A.M., Manceau, A., Schlegel, M.L., Baeyens, B., Bradbury, M.H., Morales, M., 2002.
322 Neoformation of Ni phyllosilicate upon Ni uptake on montmorillonite: A kinetics study by powder and polarized
323 extended X-ray absorption fine structure spectroscopy. Geochim. Cosmochim. Acta 66, 2335–2347.

324 Dazas, B., Lanson, B., Breu, J., Robert, J.-L., Pelletier, M., Ferrage, E., 2013. Smectite fluorination and its impact on
325 interlayer water content and structure: A way to fine tune the hydrophilicity of clay surfaces? Microporous
326 Mesoporous Mater. 181, 233–247.

327 Elam, W.T., 1989. X-ray absorption. Edited by D. C. Koningsberger and R. Prins. Published by John Wiley and Sons, New
328 York, 1988; price $77.50, ISBN 0-471-87547-3. X-Ray Spectrom. 18, 41.

329 Gates, W.P., 2006. Chapter 12.3 X-ray Absorption Spectroscopy, in: Faïza Bergaya, B.K.G.T. and G.L.B.T.-D. in C.S. (Ed.),
330 Handbook of Clay Science. Elsevier, pp. 789–864.

331 Gates, W.P., Bordallo, H.N., Aldridge, L.P., Seydel, T., Jacobsen, H., Marry, V., Churchman, G.J., 2012. Neutron Time-of-
332 Flight Quantification of Water Desorption Isotherms of Montmorillonite. J. Phys. Chem. C 116, 5558–5570.

333 Ghadiri, M., Hau, H., Chrzanowski, W., Agus, H., Rohanizadeh, R., 2013. Laponite clay as a carrier for in situ delivery of
334 tetracycline. RSC Adv. 3, 20193–20201.

335 Gräfe, M., Nachtegaal, M., Sparks, D.L., 2004. Formation of metal-arsenate precipitates at the goethite-water
336 interface. Environ. Sci. Technol. 38, 6561–70.

337 Gräfe, M., Sparks, D.L., 2005. Kinetics of zinc and arsenate co-sorption at the goethite–water interface. Geochim.
338 Cosmochim. Acta 69, 4573–4595.

339 Grassi, G., Michels, L.E., Jr., R.D., Gholamipour-Shirazi, A., Aalerud, T., Knudsen, K.D., Fossum, J.O., Silva, G.J. da, 2013.
340 Intercalation processes in clay mineral: Synthetic Ni-Fluorohectorite.

341 Hansen, E.L., Hemmen, H., Fonseca, D.M., Coutant, C., Knudsen, K.D., Plivelic, T.S., Bonn, D., Fossum, J.O., 2012.
342 Swelling transition of a clay induced by heating. Sci. Rep. 2.

343 Hemmen, H., Rolseth, E.G., Fonseca, D.M., Hansen, E.L., Fossum, J.O., Plivelic, T.S., 2012. X-ray Studies of Carbon
344 Dioxide Intercalation in Na-Fluorohectorite Clay at Near-Ambient Conditions. Langmuir 28, 1678–1682.

345 Hofmann, U., Klemen, R., 1950. Verlust der Austauschf$\blacklozenge$higkeit von Lithiumionen an Bentonit durch Erhitzung.
346 Zeitschrift f$\blacklozenge$ Anorg. Chemier Anorg. Chemie 262, 95–99.

Komadel, P., 1999. Structure and Chemical Characteristics of Modified Clays, in: Misaelides, P., Macášek, F., Pinnavaia, T.J., Colella, C. (Eds.), Natural Microporous Materials in Environmental Technology SE - 1, NATO Science Series. Springer Netherlands, pp. 3–18.

Komadel, P., Madejová, J., Bujdák, J., 2005. Preparation and properties of reduced-charge smectites – a review. Clays Clay Miner. 53, 313–334.

Kreit, J.F., Shainberg, I., Herbillon, A.J., 1982. Hydrolysis and decomposition of hectorite in dilute salt solutions. Clays Clay Miner. 30, 223–231.

Lee, P.A., Beni, G., 1977. New method for the calculation of atomic phase shifts: Application to extended x-ray absorption fine structure (EXAFS) in molecules and crystals. Phys. Rev. B 15, 2862–2883.

Lee, P.A., Pendry, J.B., 1975. Theory of the extended x-ray absorption fine structure. Phys. Rev. B 11, 2795–2811.

Løvoll, G., Sandnes, B., Méheust, Y., Måløy, K.J., Fossum, J.O., da Silva, G.J., Mundim, M.S.P., Droppa Jr., R., Fonseca, D.M., 2005. Dynamics of water intercalation fronts in a nano-layered synthetic silicate: A synchrotron X-ray scattering study. Phys. B Condens. Matter 370, 90–98.

Manceau, A., Schlegel, M.L., Baeyens, B., Bradbury, M.H., 2003. Neoformation of Ni phyllosilicate upon Ni uptake on montmorillonite : A kinetics study by powder and polarized extended X-ray absorption fine structure spectroscopy 67.

Michels, L.E., Hemmen, H., Jr., R.D., Grassi, G., Silva, G.J. da, Fossum, J.O., 2012. Synchrotron X-ray scattering studies of Li-Fluorohectorite synthetic clay: Random intercalation states. Proc. 2nd Int. Work. Complex Phys. Phenom. Mater. 1, 32–34.

Newville, M., 2001. EXAFS analysis using FEFF and FEFFIT. J. Synchrotron Radiat. 8, 96–100.

O'Day, P.A., Rehr, J.J., Zabinsky, S.I., Brown, G.E.J., 1994. Extended X-ray Absorption Fine Structure (EXAFS) Analysis of Disorder and Multiple-Scattering in Complex Crystalline Solids. J. Am. Chem. Soc. 116, 2938–2949.

Pandya, K.I., O'Grady, W.E., Corrigan, D.A., McBreen, J., Hoffman, R.W., 1990. Extended x-ray absorption fine structure investigations of nickel hydroxides. J. Phys. Chem. 94, 21–26.

Ravel, B., 2001. ATOMS : crystallography for the X-ray absorption spectroscopist. J. Synchrotron Radiat. 8, 314–316.

Ravel, B., Newville, M., 2005. ATHENA, ARTEMIS, HEPHAESTUS: data analysis for X-ray absorption spectroscopy using IFEFFIT. J. Synchrotron Radiat. 12, 537–41.

Ribeiro, L., Mundim, M.S.P., Silva, G.. da, Fossum, J.O., Mundim, K.C., 2007. Temperature investigation of intercalation and diffusion processes in synthetic nanosilicates by means of synchrotron X-ray absorption spectroscopy. J. Electron Spectros. Relat. Phenomena 156, 4–6.

377 Ribeiro, L., Silva, G.J. da, Mundim, M.S.P., Sousa, M.H., Fossum, J.O., Mundim, K.C., 2011. Estudo dos Processos de
378 Intercalação de Água em Nanosilicatos Sintéticos Utilizando Radiação Síncrotron. Rev. Process. Químicos 5, 56–
379 74.

380 Sandstrom, D.R., Dodgen, H.W., Lytle, F.W., 1977. Study of Ni(II) coordination in aqueous solution by EXAFS analysis. J.
381 Chem. Phys. 67, 473.

382 Sayers, D.E., Stern, E.A., Lytle, F.W., 1971. New Technique for Investigating Noncrystalline Structures: Fourier Analysis
383 of the Extended X-Ray—Absorption Fine Structure. Phys. Rev. Lett. 27, 1204–1207.

384 Schaich, W.L., 1973. Comment on the Theory of Extended X-Ray-Absorption Fine Structure. Phys. Rev. B 8, 4028–4032.

385 Scheckel, K.G., Scheinost, A.C., Ford, R.G., Sparks, D.L., 2000. Stability of layered Ni hydroxide surface precipitates—a
386 dissolution kinetics study. Geochim. Cosmochim. Acta 64, 2727–2735.

387 Scheidegger, A.M., Lamble, G.M., Sparks, D.L., 1996. Investigation of Ni Sorption on Pyrophyllite: An XAFS Study.
388 Environ. Sci. Technol. 30, 548–554.

389 Scheinost, A., Sparks, D., 2000. Formation of Layered Single- and Double-Metal Hydroxide Precipitates at the
390 Mineral/Water Interface: A Multiple-Scattering XAFS Analysis. J. Colloid Interface Sci. 223, 167–178.

391 Tenorio, R.P., Alme, L.R., Engelsberg, M., Fossum, J.O., Hallwass, F., 2008. Geometry and dynamics of intercalated
392 water in Na-fluorhectorite clay hydrates. J. Phys. Chem. C 112, 575–580.

393 Tenorio, R.P., Engelsberg, M., Fossum, J.O., Da Silva, G.J., 2010. Intercalated Water in Synthetic Fluorhectorite Clay.
394 Langmuir 26, 9703–9709.

395 Tolentino, H., Cezar, J.C., Cruz, D.Z., Compagnon-Cailhol, V., Tamura, E., Martins Alves, M.C., 1998. Commissioning and
396 first results of the LNLS XAFS beamline. J. Synchrotron Radiat. 5, 521–3.

397 Tolentino, H.C.N., Ramos, A.Y., Alves, M.C.M., Barrea, R.A., Tamura, E., Cezar, J.C., Watanabe, N., 2001. A 2.3 to 25 keV
398 XAS beamline at LNLS. J. Synchrotron Radiat. 8, 1040–1046.

399 Wada, N., Hines, D.R., Ahrenkiel, S.P., 1990. X-ray-diffraction studies of hydration transitions in Na vermiculite. Phys.
400 Rev. B 41, 12895–12901.

401 Wang, J., Kalinichev, A.G., Kirkpatrick, R.J., 2004. Molecular modeling of water structure in nano-pores between
402 brucite (001) surfaces. Geochim. Cosmochim. Acta 68, 3351–3365.

403